01 Dec 2019

Design And Sensitivity Analysis Of EBG Stripline Common-Mode Filters

Marina Y. Koledintseva
Missouri University of Science and Technology, marinak@mst.edu

Sergiu Radu

Joseph Nuebel

Recommended Citation

M. Y. Koledintseva et al., "Design And Sensitivity Analysis Of EBG Stripline Common-Mode Filters," *IEEE Transactions on Electromagnetic Compatibility*, vol. 61, no. 6, pp. 1746 - 1759, article no. 8621047, Institute of Electrical and Electronics Engineers, Dec 2019.
The definitive version is available at https://doi.org/10.1109/TEMC.2018.2889441

Design and Sensitivity Analysis of EBG Stripline Common-Mode Filters

Marina Y. Koledintseva, *Senior Member, IEEE*, Sergiu Radu, *Senior Member, IEEE*, and Joseph Nuebel, *Member, IEEE*

***Abstract*—Workflow of electromagnetic bandgap (EBG) common-mode (CM) filter design of edge-coupled differential pairs on a printed circuit board (PCB) and sensitivity of its characteristics to variations of geometrical and material parameters are discussed. A number of simple 20-GHz EBG CM notch filters for differential stripline pairs are designed using full-wave numerical electromagnetic modeling, fabricating, and testing. The cases of one and two stripline differential pairs crossing the EBG patches are considered. The modeled and measured mixed-mode *S*-parameters are analyzed as functions of geometrical parameters, including size and number of EBG patches, gaps between them, geometry and position of signal traces across the EBG patches, and thicknesses of dielectric layers. The agreement between the measured and modeled mixed-mode *S*-parameters validates the models and allows for further numerical experiments. It is shown that the EBG filter performance depends on various subtle technological features, e.g., conductor surface roughness on metal surfaces; length imbalance on a differential pair; rate of coupling of lines within each differential pair and between the pairs; and some other factors. The systematic analysis of the trends for filter characteristics as functions of various design parameters allows for an optimal design of the CM notch filter.**

***Index Terms*—Bandwidth, common mode (CM), conductor surface roughness, differential mode (DM), differential pair, electromagnetic bandgap (EBG) structure, full-wave numerical electromagnetic modeling, notch filter, *S*-parameters, stripline, vector network analyzer.**

I. Introduction

PERIODIC microwave, or electromagnetic bandgap (EBG) structures, synonymic to photon crystals when scaling from optics to microwaves and radio frequencies, are known to comprise frequency-selective surfaces and passive narrowband bandstop and passband filters [1]–[7]. A common-mode (CM) filter at the input/output (I/O) of high-speed digital electronics designs is one of the examples of practical use of EBG structures for mitigating unwanted electromagnetic emissions [8], [9]. I/O CM filters based on discrete components and/or ferrites cannot operate at frequencies above a few GHz, whereas EBG filters can work at much higher frequencies and can be directly integrated into the printed circuit board (PCB) layout based on the standard multilayer PCB technology. A preferable EBG filter design should be without extra vias—the latter may compromise the signal integrity (SI).

As data rates in digital designs increase, there is a necessity in increasing the notch frequencies of CM filters. The advantages of EBG filters justify the necessity of a thorough analysis in order to optimize the design workflow and analyze the technological variables at very high frequencies, where they are more difficult to control and simulate.

There are a number of publications on the modeling and design of various planar EBG structures on PCBs for high-speed digital applications—see, e.g., [8] and references therein. There are two groups of problems EBG filters can solve. The first group is related to power bus noise reduction (this is beyond the scope of the present paper), and the second group is the mitigation of CM currents from I/Os on PCBs and cables attached [9]–[14]. There are studies on EBG structures used to suppress CM at selected frequencies in differential microstrip and striplines: at 4.5 [11], 5, and 7.5 GHz [12], [13]. The 8-GHz removable planar microstrip EBG CM filter that contains square patches connected by thin bridges is described in [8]. A dual-band filter for 2.5 and 4.5 GHz is reported in [14], and more high-frequency dual-band filter, for 10.3 and 20.6 GHz, is presented in [15].

The basic physical principle of an EBG filter operation in a majority of cases is comparatively simple. A periodic patterned structure comprised of identical (or nearly identical) EBG cavities resonates at a number of discrete frequencies determined by the geometry of an EBG patch.

If a patch is rectangular, as is illustrated by Fig. 1, the resonances will appear at the frequencies analogous to those for a rectangular cavity [16]

$$f_{mn0} = \frac{c}{2\sqrt{\varepsilon_r}}\sqrt{\left(\frac{m}{A_x}\right)^2 + \left(\frac{n}{A_y}\right)^2 + \left(\frac{k}{A_z}\right)^2}, \quad (1)$$

where c is the speed of light in free space; ε_r is the relative permittivity of the dielectric medium; $A_{x,y,z}$ are the dimensions of the EBG patch along the corresponding x, y, z axes; and m, n, k are the numbers of half-wavelength variations of E-field along the corresponding dimensions of the EBG patch. Since a PCB EBG structure is typically two-dimensional (2-D), with thickness (z-dimension) of a PCB dielectric between the signal and EBG layers being much smaller than the other two

Manuscript received October 16, 2018; revised November 23, 2018 and December 13, 2018; accepted December 17, 2018. Date of publication January 22, 2019; date of current version December 27, 2019. This work was supported in part by Oracle Corp., USA. *(Corresponding author: Marina Y. Koledintseva.)*

M. Y. Koledintseva was with Oracle Corporation, Santa Clara, CA 95054 USA. She is now with Metamagnetics, Inc., Westborough, MA 01581-1087 USA (e-mail: mkoledintseva@mtmgx.com).

S. Radu and J. Nuebel are with Oracle Corporation, Santa Clara, CA 95054 USA (e-mail: sergiu.radu@oracle.com; joe.nuebel@oracle.com).

Color versions of one or more of the figures in this paper are available online at http://ieeexplore.ieee.org.

Digital Object Identifier 10.1109/TEMC.2018.2889441

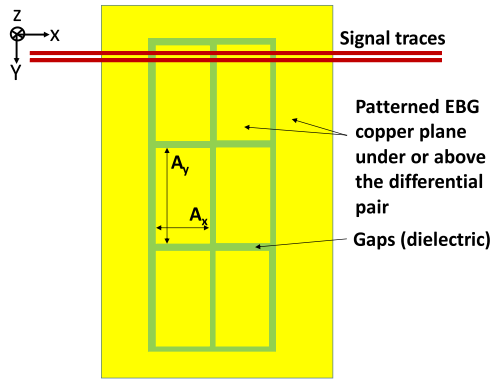

Fig. 1. Differential pair running on a signal layer across the rectangular patterned EBG on the return plane.

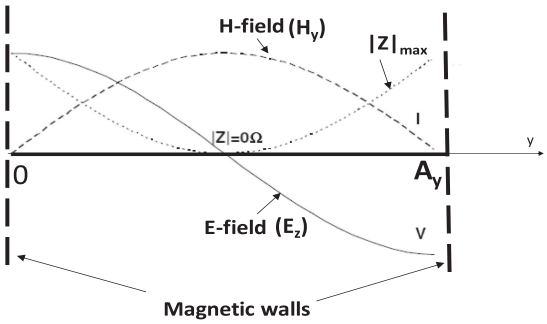

Fig. 2. Field variation along *y* for TM_{010} mode in an EBG patch.

dimensions, the third term in (1) can be omitted. If one of the dimensions in the PCB plane is such that the corresponding size is cutoff, then only the other dimension would play a part at the resonance.

Let us consider an EBG structure excited by a differential pair running along *x*-direction so that the differential pair crosses the periodic EBG structure consisting of stripes narrow in *x*-dimension and extended in *y*-dimension. If *x*-dimension of an EBG patch is cutoff, and *y*-dimension fits one electromagnetic field variation at the desirable CM notch frequency, then the mode TM_{010} is excited in each cavity comprised of a patch with magnetic walls at the gaps and a return (ground) plane. The E_z field component between an EBG patch and the return plane varies as $E_z \sim \cos(\pi y/A_y)$ [17]. This is illustrated by Fig. 2. This field variation determines where a differential pair should run across *y*-dimension to most effectively excite the EBG structure. Obviously, it should be closer to the edges and not in the center.

The electromagnetic field of CM is concentrated in the space between the signal trace and the return plane that is patterned. This CM field at the EBG resonance frequency will be the most effectively coupled into the space between the EBG layer and the return plane under it through the gaps surrounding the EBG structure and between the patches. In other words, a patch cavity at the resonance appears as very low impedance to the return (ground) plane, and thus is equivalent to a bandstop notch filter.

While CM is significantly damped at the resonance (CM filter notch) frequency, the differential mode (DM) associated with signal transmitted along the differential pair, remains intact. This happens because the electromagnetic field of the DM is mainly concentrated between the signal traces. The gap sizes, together with the dimensions of patches and their number, determine the overall size of the EBG structure and space it occupies on the PCB. But gaps may also affect EBG filter performance. If the differential pair running along the *x*-direction crosses g_x gaps that are negligibly small compared to the wavelength, and the traces are at a height larger than the gap, there is practically no distortion of the DM. Obviously, if gaps g_x were wide enough, their impact on the DM would have increased. At the same time, the g_x size may affect the CM over the frequency range of interest, as traces over gaps are a known issue for single-ended traces and for CM in differential pairs. The wider gap g_x will help the CM "absorption" by forcing more CM field into the region between the EBG structure and the ground plane next to the EBG layer. The gaps g_y between the EBG rows practically do not affect DM propagation; however, the gap g_y has an impact on the coupling between the individual patches and therefore may affect the depth and the width of the designed EBG CM notch filter.

In literature, there is much attention paid to microstrip EBG structures, i.e., where signal traces are on the top or bottom of a PCB, and the patterned EBG layer is the next in the stackup—see [8], [13] and references therein. In [18], physical and technological aspects of microstrip EBG CM filters designs are discussed, and CM notch filters for 19.2 GHz are modeled considering various technological features (frequency-dispersive PCB substrate dielectric, solder mask, conductor surface roughness, trapezoid shape of traces, and length imbalance of traces). The modeled microstrip EBG filters are implemented on a PCB, and there is a good agreement between the measured and modeled mixed-mode parameters.

Along with microstrip EBG filters, there are also publications on the design of stripline EBG filters [15], [19]–[22]. Filtering of CM on the differential pairs located on the inner layers of PCBs may be preferable in high-density designs for space-optimization purposes. Also, a majority of high-speed differential networks, especially operating at multi-gigabit per second speeds, are routed as striplines on the inner layers rather than microstrips on the outer layers. This is done for both SI and EMC purposes due to the better electromagnetic field containment in stripline structures than in microstrip. Near the locations where differential pairs change layers, e.g., from stripline to microstrip, or where inhomogeneities and imbalances due to transitions to connector pins are, stripline EBG filters may help to reduce unwanted CM as a source of EMI.

However, in the existing publications, there is very little information about design of stripline filters for tens of gigahertz. In [19] and [21], the dual-band (8 and 16 GHz) stripline filter is considered; in [20], the stripline filters for 14–15 GHz are presented. This paper [15] describes dual 10.3 and 20.6 GHz EBG filter design that can be both microstrip and stripline; however, there is no analysis of technological peculiarities of designing such filters since the presented EBG structures are pretty complex, and their implementation is not straightforward, especially at 20.6 GHz.

In this paper, the possibility of increasing operating frequency of stripline CM EBG filters is considered. The EBG patches of rectangular shape are chosen for simplicity of implementation on a PCB. Similar to the case of microstrip EBG filters [18], technological limitations that can affect the center frequency and the shape of the filter response will be discussed. It is important that such a filter does not compromise the propagation of the DM on the signal pair. Therefore, mixed-mode *S*-parameters to characterize such filters will be used.

In this particular work, a number of 20-GHz EBG CM notch filters for differential striplines lines were first modeled numerically, then implemented in a PCB, and tested experimentally. This study is motivated by the necessity of such EBG filters for high-speed interfaces in server designs.

Note that the frequency of 20 GHz of the CM EBG filter design presented herein is high enough that all conceivable design variables matter, therefore the detailed sensitivity analysis is provided and can be referenced when designing filters for the other frequencies.

The methodology of EBG filters design is described in Section II. Herein, the optimal design workflow for EBG filters operating at around 20 GHz is analyzed. However, the methodology for the design of the filters for the other frequencies is the same. The test scenarios and measurement setup are described in Section III. The EBG filters in this paper have been designed for one and two differential pairs passing through the same EBG structure. In the first case, the four-port *S*-parameter network was tested, and in the second case, the eight-port network. The modeled and measured single-ended *S*-parameters in both cases were converted to the mixed-mode *S*-parameters. In principle, more than two differential pairs may cross one EBG structure; this will make the filter response more complex due to coupling of more resonance structures with close but different resonance frequencies; however, such analysis is beyond the scope of the present paper. The comparison between the modeled and measured results is given in Section IV. Section V shows the basic trends when varying different design parameters of EBG filters in the numerical models.

II. Stripline EBG CM Filter Physics and Design

Physics of the CM filtering using the microstrip and stripline EBG structures have much in common, and yet they are different, because the stripline consists of two reference planes, whereas microstrip has only one. In the microstrip EBG structure, the return plane with EBG pattern allows for some current fringing through the gaps and flowing on the solid ground plane beneath the EBG layer. This comprises periodic cavities limited by magnetic walls between the EBG layer and the solid ground plane, and these cavities are excited by signal traces running above the EBG patches.

In the case of the stripline structure, EBG patterns can be either on both return planes (above and beneath the signal traces) or on one of them, e.g., beneath the traces only. In the case of the one-sided EBG, there will be two groups of coupled cavities. The first group is formed by the first ground plane and the EBG patches next to it and does not include the signal traces, and

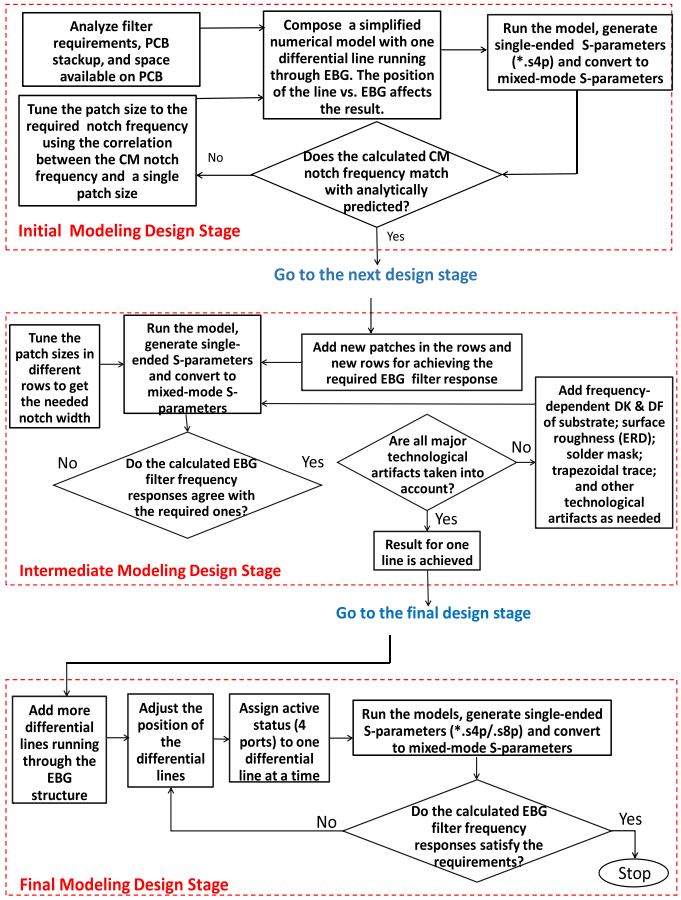

Fig. 3. Workflow for EBG filter design: initial, intermediate, and final stages.

the second group is formed between the EBG and the other ground plane and includes the signal layer. In the case of the two-sided EBG, there will be three groups of coupled cavities. Two groups are between the EBG and the closest ground plane to them, and the third group is comprised of cavities between two EBG structures that include the signal layer.

Obviously, the structures with two or three coupled cavities in the stripline cases are more complex than the two-cavity microstrip structure, and there are more degrees of freedom to control the CM notch frequency, shape, depth, and width at a certain level.

Fundamental behavior of any planar EBG structure depends on its geometry and materials. Major factors having impact on the CM notch filter characteristics include patch dimensions, number of patches in both directions on the PCB, distances between patches, position of traces exciting the EBG, and PCB substrate thickness. Secondary factors are the geometry of differential lines, rate of their coupling, and various PCB technological features, including frequency-dispersive PCB matrix dielectrics, both core and prepreg, solder mask, trapezoid shape of signal traces, conductor surface roughness on signal traces and return planes, including EBG patches, and length imbalance on differential pairs.

The general workflow for EBG CM filter design is illustrated by Fig. 3. At the initial design stage, a simplified model with

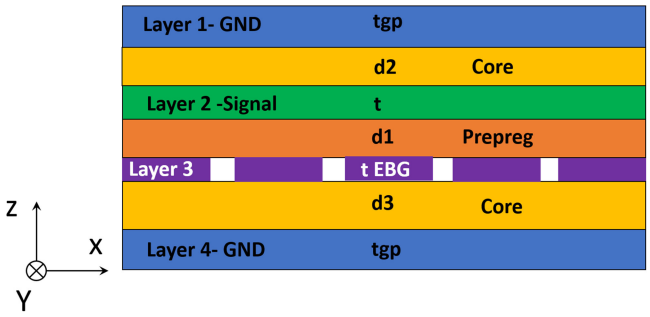

Fig. 4. Stackup of a single-sided stripline EBG structure.

only basic parameters affecting CM notch filter characteristics is developed. The intermediate stage is the stage when tuning of the model to the required CM filter parameters is done by changing the number of patches, slightly modifying their dimensions, placement of the differential pair across the EBG pattern, and adding various technological features. At this stage, only one differential pair is considered. At the final stage, more differential pairs are added, and their mutual position and position with respect to EBG patches is tuned to obtain the best possible CM filtering result.

Not losing generality of the design methodology, the study presented herein is limited by a single-sided EBG. A cross-section of such an EBG structure with a stripline differential pair is shown in Fig. 4.

In this case, the differential pair is located on Layer 2, the EBG structure is directly under the differential pair on Layer 3, and Layer 4 is the lower solid ground (GND) plane under the EBG. The upper GND plane is on Layer 1. The EBG patches on Layer 3 and GND on Layer 4 form a cavity with magnetic walls which will resonate at frequencies related to the EBG patches geometry and properties of the dielectric filling the cavity. This resonance results in electromagnetic energy absorption mainly from the CM due to the field structure of the latter between the signal traces and the return plane. At the same time, the DM is almost unaffected since its electromagnetic fields are mainly concentrated in the space between the traces, practically not penetrating into the region between Layers 3 and 4.

As is seen in Fig. 4, there is another cavity—between EBG layer (Layer 3) and the top Layer 1 with signal traces run in between on Layer 2 and inhomogeneous dielectric, if core (*d2*) and prepreg (*d1*) are different. The resonances in this inhomogeneous cavity are excited by the traces and couple with the lower cavity filled by dielectric *d3*. Due to this coupling of two cavities, the resonance behavior is expected to be different from the one in the microstrip EBG structure: The CM notch may shift and change its shape.

This is briefly the physical mechanism of the CM notch filtering at the patch resonance frequency in the case of the stripline EBG filter. The CM notch filter center frequency is governed by formula (1). Herein, it is assumed that the z-axis is perpendicular to the PCB plane, x is the axis along the differential pair, and y is, correspondingly, across it. Since the distances along the z-direction between the planes in PCB stackup (herein, Layers 3 and 4 for the lower cavity, and between Layers 3 and 1 for the upper cavity) are much smaller than half of the wavelength in the dielectric medium, there are no variations of the field along z-direction.

Therefore, only 2-D resonances due to the x and y dimensions are of importance for CM propagation on the microstrip differential pair, and the resonant modes inside *each* thin cavity associated with an *individual* rectangular patch are of TM_{010} type, having the resonance frequencies (1). Assume that signal traces run along the x-axis, and the dimension A_x is cutoff for any E-field variations over the frequency range of interest, and the only dimension of EBG that determines the resonance frequency of EBG patches is A_y.

For a 2-D EBG structure consisting of a number of identical (or nearly identical) patches along x and y, there is a superposition effect of all the patches on the CM mode. Obviously, the more patches in a row a differential pair crosses along the propagation x-direction, the more damping of the CM is expected, and the deeper the CM filter notch will be. However, there is coupling between individual patches if they are approximately of the same dimensions. Resonance from one patch "propagates" outside the magnetic walls of the initial cavity and excites resonances in the other patches if properly dimensioned. Therefore, the CM notch will also be affected by the patches not directly crossed by the signal traces. Due to the multiple gaps in the EBG structure, there is still coupling between the traces and more distant patches. The number of patches and the sizes of the gaps between them affect the coupling with the signal traces and therefore the depth and width of the CM filter. Due to resonance loading effect with more patches, the resonance frequency may slightly shift to the lower frequencies. Placing more patches in the column leads to the deeper notch.

The center frequency of the notch, depth, and width depend on the variation in the dimensions of the individual patches, as well as the other factors, such as dielectric and copper properties on the PCB. For many practical applications, the wider CM notch may be desirable; too narrow of a notch may result in missing the frequency that needs rejection. Introducing any structural aperiodicity, or unequal dimensions of the patches within the EBG, will result in the broader notch. For example, in [8], unequal sizes of the EBG cells (varying along the propagation x-direction) were considered to increase the bandwidth of the EBG notch filter. The similar effect could be reached by keeping all x-dimensions of the patches identical, varying only y sizes of the patches [18]. This is the way to broaden the notch if it is the y-dimension that determines the resonance frequency of the structure, while x-dimension is too small to allow the E-field variations over the frequency range of the filter operation. Variation of gaps between the patches also results in a broader CM notch.

An EBG structure with signal traces running over it is schematically shown in Fig. 5. In this figure, 2×4 EBG structure is shown as an example, but there may be a different number of patches. In the general case, all patches have different dimensions A_{xi} and A_{yj}, where indices i and j show the position of a patch in the EBG structure, corresponding to a column number

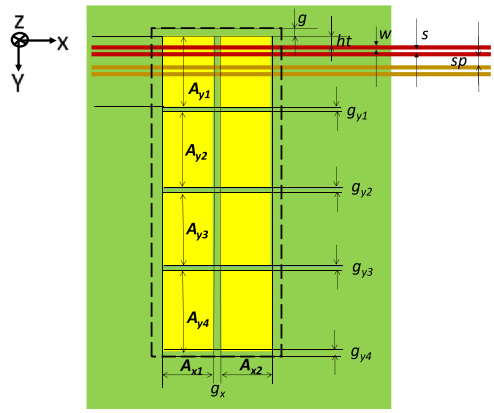

Fig. 5. Schematic of EBG structure and differential pairs running across it (copper beyond the dashed line of EBG frame is not seen, but present).

and a row number, respectively. In a real design, some of the dimensions may be identical. Similarly, gap sizes g_{xi}, g_{yj} may be either different, or the same. The distance between the top of the first row of EBG and the top edge of the first line in a differential pair is *ht*. Widths of the traces are *w*; edge-to-edge separation distance between them is *s*—and the lines may be either loosely coupled, or strongly coupled. If there are two or more differential pairs running across the EBG structure, the distance *sp* determines edge-to edge separation between the two differential pairs (from the second line of the first pair to the first line of the second pair). In the general case, there may be more than two differential pairs running through the EBG, and they do not necessarily need to be equidistant from each other.

The CM filter operation strongly depends on where the signal traces exciting the EBG structure run with respect to the patches since this determines spatial distribution and intensity of mode excitation in the EBG cavities, as is discussed above and illustrated by Fig. 2.

It will be shown below that there is an optimum position of the traces *ht* with respect to the top edge of patches in the top row, or in the subsequent rows. As is shown for the microstrip structure in [18], when the traces cross the patch in the middle of *y*-dimension (at $A_y/2$), the coupling between the differential pair and EBG structure is low, and the notch depth is minimal. In each geometry of the EBG structure, the optimal position of the traces to provide the deepest notch by achieving the most effective excitation of the resonance in the patch and the most effective coupling, is individual. For example, in the EBG structure with one row of multiple patches with only the A_y dimension playing the part, the positions of differential pairs around $A_y/4$ appear to be the most effective from the point of view of getting the deeper notch. For stripline EBG filters, the trends of the CM notch filter parameters behavior with *ht* variation are expected to be close to those for a microstrip structure, but not necessarily the same. The positions of optimal excitation may be affected by coupling with the resonances from the second cavity which is above the EBG structure.

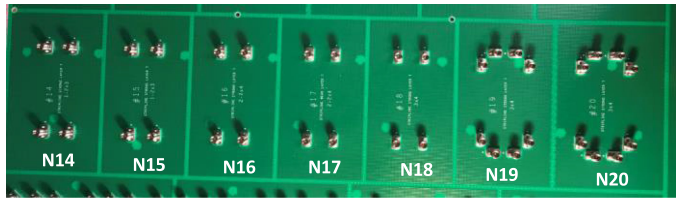

Fig. 6. Test board with EBG stripline scenarios: ##14–18 (or N14–N18) with one and #19 (N19) and #20 (N20) with two differential pairs.

TABLE I
GEOMETRICAL FEATURES OF EBG STRUCTURES AND DIFFERENTIAL PAIRS

Test board name	Number of diff. pairs	EBG structure *x* x *y*	gx=gy, mm	*w*, mm	*s*, mm	*sp*, mm
N14	1	2x3	0.25	0.094	0.110	-
N15	1	2x3	0.39	0.094	0.110	-
N16	1	2x4	0.25	0.094	0.110	-
N17	1	2x4	0.25	0.107	0.183	-
N18	1	3x4	0.25	0.094	0.110	-
N19	2	3x4	0.25	0.094	0.110	0.360
N20	2	3x4	0.25	0.094	0.110	1.305

III. TEST BOARD DESCRIPTION AND MEASUREMENT SETUP

A test board with a number of EBG filters was designed and fabricated. Its fragmented seven test scenarios with stripline differential pairs are shown in Fig. 6. It contains five structures (N14-N18) with one differential pair crossing the EBG pattern, and two structures (N19 and N20) with two differential pairs crossing the corresponding EBG patterns. The structures N14 and N15 contain 2 × 3 patches in EBG, the structures N16 and N17 contain 2 × 4 patches, and structures N18-N20 contain 3 × 4 patches. The geometrical differences between the structures are summarized in Table I. The common parameters are the following. The distance between the top edge of EBG pattern and the top of the first line in each differential pair is $ht = 0.472$ mm. The EBG patch sizes in the manufactured test board are the following. Their *x*-dimension is $A_{x1} = A_{x2} = 1.91$ mm in all the patches; their *y* dimensions in the corresponding rows are $A_{y1} = 3.60$ mm, $A_{y2} = 3.65$ mm, $A_{y3} = 3.74$ mm, and $A_{y4} = 3.80$ mm. The size of the first patch (3.60 mm) basically determines the CM notch frequency at ∼20 GHz. The different *y* sizes provide the wider CM notch of the designed EBG filters.

The test board was a ten-layer PCB; the differential pairs were implemented on Layer 7. EBG structure was on Layer 8, and Layers 6 and 9 were solid ground planes. Coaxial 2.92-mm connectors were surface-mounted on top Layer 1. Layers 7 and 8 were 1-oz, and Layers 6 and 9 were 0.5-oz standard (STD) copper. PCB dielectric was Megtron 6. All the differential pairs were about 80.4 ± 0.25 mm long (or ∼3.165 in) and had differential impedance $Z_{DM} = 100\,\Omega$, and CM impedance Z_{CM} close to 25 Ω, with ±10% possible deviation from the nominal values.

The single-ended and mixed-mode *S*-parameters of the differential lines crossing the EBG structures were measured using

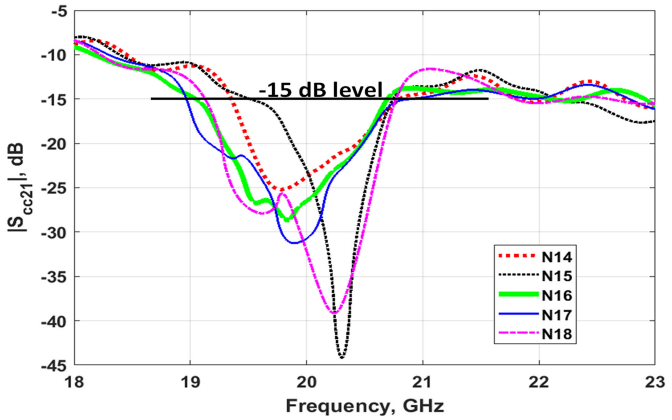

Fig. 7. CM notch filter frequency response with one differential pair crossing EBG.

Agilent Technologies (Keysight) vector network analyzer PNA N5225 A, operating over the frequency range 10 MHz–50 GHz. However, measurements were done only up to 26 GHz since this was the frequency range of interest for the designed 20-GHz filters. Calibration was done using Keysight N4692 A Electronic Calibration module (E-cal).

A. EBG Structures Crossed by One Differential Pair

The measured frequency characteristics for CM notch filters N14–N18 with one differential pair crossing EBG structures are shown in Fig. 7. Typically, the CM rejection bandwidth at some level is evaluated around the notch frequency. Herein, the bandwidth at the level of –15 dB is of interest at 20 GHz. What is below that level is not critical for the CM EBG filter performance. The desired bandwidth of about 1 GHz was determined by the specific application of EBG CM in our multi-socket server design.

The directly measured OFF-resonance insertion loss (IL) for CM varies from ∼8 to ∼15 dB over the frequency range 18–23 GHz in all the test scenarios. However, this loss includes port effects associated with 1-mm long via stubs when signal traces are on Layer 7. When port effects are removed using de-embedding procedure for differential pairs, the CM OFF-resonance IL reduces to ∼5–8 dB over the same frequency range. The directly measured IL for DM varies almost linearly from 6 to 9 dB for the range 18–23 GHz; and when port effects are de-embedded, $|S_{dd21}|$ is about –4 dB at 18 GHz and –6 dB at 23 GHz. The resultant mode conversion is below –20 dB over the frequency range of interest for all the test scenarios. The data is summarized in Table II.

Note the distortion of shapes of frequency characteristics of all the CM filters, except for N15. Various EBG patches have slightly different dimensions, which causes overlapping and widening the notch, and this is true for all the designed herein EBG structures. The difference between N15 and the other structures is that the gap size in N15 is $g_x = g_y = 0.39$ mm, whereas in the other structures it is 0.25 mm. The narrower gap causes an increased coupling between individual EBG cavities and additional splitting of resonances. Therefore, N15 having the best frequency characteristic is chosen as a baseline structure for the further analysis and comparison with the modeled results.

TABLE II
MEASURED PARAMETERS OF CM EBG FILTERS

Test board name	Notch freq., GHz	Notch magnitude, dB	Rejection band, GHz @ -20dB	Rejection band, GHz @ -15 dB	Mode conversion, dB @ 20GHz
N14	19.78	-25.20	0.93	1.50	-31.60
N15	20.29	-44.05	0.75	1.40	-21.60
N16	19.85	-28.82	1.21	1.65	-24.18
N17	19.92	-31.27	1.32	1.95	-26.03
N18	20.22	-39.38	1.42	1.75	-27.97
N19	18.88 20.55	-28.10 -38.84	1.95	2.20	-20.22
N20	19.35 20.38	-43.02 -31.86	1.48	1.75	-23.84

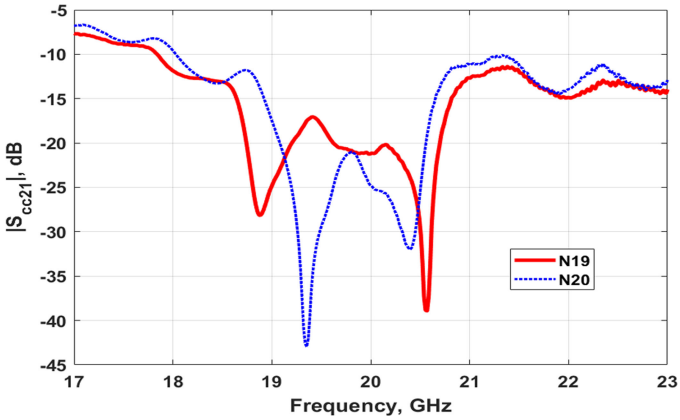

Fig. 8. CM notch filter frequency response with two differential pairs crossing the EBG structure.

B. EBG Structures Crossed by Two Differential Pairs

The measured frequency characteristics for the filters N19 and N20 with two differential pairs crossing the EBG are shown in Fig. 8. The parameters of the filters are summarized in Table II. Since there are two minima in each frequency characteristic, their parameters (resonance frequencies and magnitudes for both minima) are included in Table II. Mode conversion for these two test scenarios are below –20 dB; OFF-resonance $|S_{cc21}|$ varies from –8 to –15 dB for N19 (or IL for CM varies from 2.52 to 4.74 dB/in) and from –6.3 to –15 dB for N20 (or IL for CM from 1.99 to 4.74 dB/in) over frequency range 18–23 GHz. The DM IL in the structure varies from 5 to 7 dB (or from 1.57 to 2.21 dB/in) over frequency range 18–23 GHz in both cases, when port effects are removed.

Two dips in the frequency characteristics are explained by the notch splitting when two differential pairs excite the same patch; this results in coupled oscillations [23]. The positions of two traces across the EBG are slightly different; this explains why the two resonances are seen apart. In the case of N19, the two differential pairs are placed closer to each other than in N20, and the coupling is stronger. This results in the lower magnitudes of dips, and frequency separation of dips is greater

than in more loosely coupled case N20. Also, the dimensions of the patches in rows in both EBG structures slightly differ, and this may cause different notch widening.

IV. Numerical Models of Test Boards and Modeling Results Validation by Measurements

The 3-D full-wave numerical electromagnetic modeling was involved during all the stages (see Fig. 3) of EBG filters design. Simulations were run using the time-domain (TD) finite-integral technique solver in CST Studio software [24]. TD simulations allow for simultaneously getting *S*-parameters over broad frequency range more efficiently than the frequency-domain (FD) solvers. Indeed, a number of the FD simulations for different structures were also run in CST, and the FD results agree well with their TD counterparts. In the numerical model, waveguide ports (with the electrical shielding option activated) were used for excitations of the stripline structures.

After the designed test boards with a number of EBG filter scenarios were manufactured, the initial numerical models were modified so that the actual PCB stackup data and geometry of differential pairs will be used in the models. This way, good agreement between the measurements and models certifies that the numerical models are adequate. Consistency in sensitivity to variations of parameters in different test scenarios and corresponding numerical models is another proof that the models describe adequately the real designs.

Various PCB-related technological features were included in models, analogous to [18], [25]. These include frequency-dispersive Megtron 6, trapezoid traces, 5–10 mil line length imbalance, and conductor roughness. In the designs, STD copper foil with its typical roughness parameters was used. There was no opportunity of directly measuring parameters of STD foil on the designed PCB, roughness parameters of the copper foil used in the PCB were evaluated as the mean values on the effective roughness dielectric (ERD) "design curves" [26] with $DK_{\mathrm{STD}} = 12$, $DF_{\mathrm{STD}} = 0.17$, and layer thickness of $tSTD = 0.0124$ mm ($\sim$0.5 mil). ERD layers were modeled on the "foil" (or matte) sides of signal traces and EBG plane, including patches.

The modeled and measured mixed-mode *S*-parameters as functions of frequency for structure N15 are compared in Figs. 9–11. In Fig. 9, IL for DM is shown. The raw measured data (dotted line) contains artifacts at the higher frequencies ($>$15 GHz) and at frequency of about 12.5 GHz. The high-frequency IL increase was due to via stub effect (length $\sim$1.01 mm); this stub was kept in order to avoid back drilling and to reduce the cost of the test board manufacturing.

Another artifact at 12.5 GHz is associated with the excitation of TE_{11} mode due to the violation of axial symmetry in the connector-via transition [27], [28]. These effects were removed by the two-port de-embedding procedure applied at each port of a differential pair, using simulations of *S*-parameters of a connector [29]. The full-wave model of the 2.92-mm connector will be considered below.

The measured result after de-embedding (port effects removed) is shown as the dashed line; however, it is still wavy at the higher frequencies. Therefore, linear approximation was used (thin solid line). The modeled result (solid thicker line) agrees well up to $\sim$15 GHz, and by 25 GHz, the difference is about 1.5 dB, which is still acceptable accuracy.

CM behavior for the same structure N15 is shown in Fig. 10 for 0–25 GHz frequency range, and in Fig. 11 zoomed in for

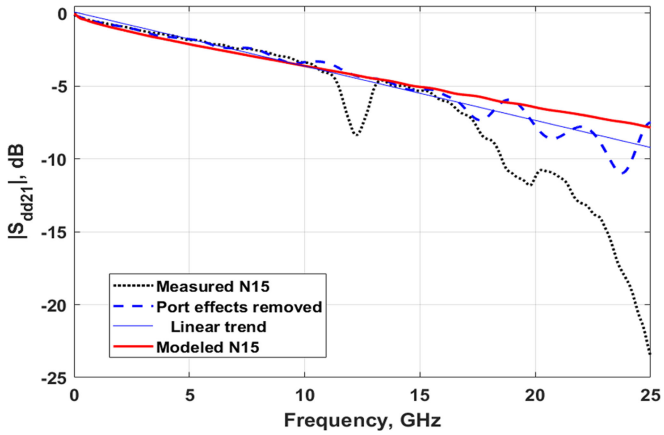

Fig. 9. Measured and modeled magnitude $|S_{dd21}|$ for DM in one differential pair crossing EBG.

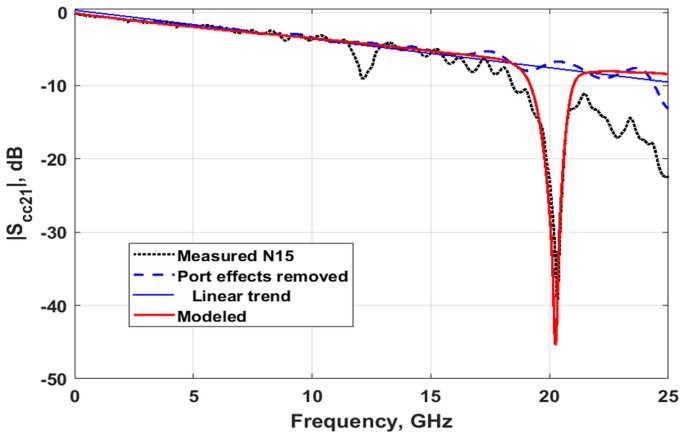

Fig. 10. Measured and modeled magnitude $|S_{cc21}|$ for CM in one differential pair crossing EBG over 0–25 GHz.

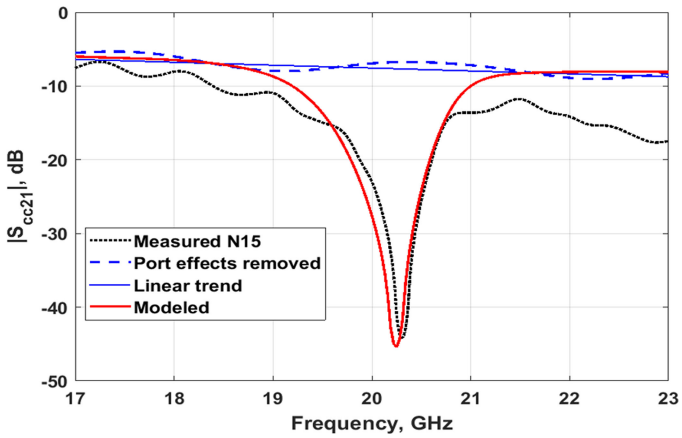

Fig. 11. Measured and modeled magnitude $|S_{cc21}|$ for CM in one differential pair crossing EBG over 16–23 GHz.

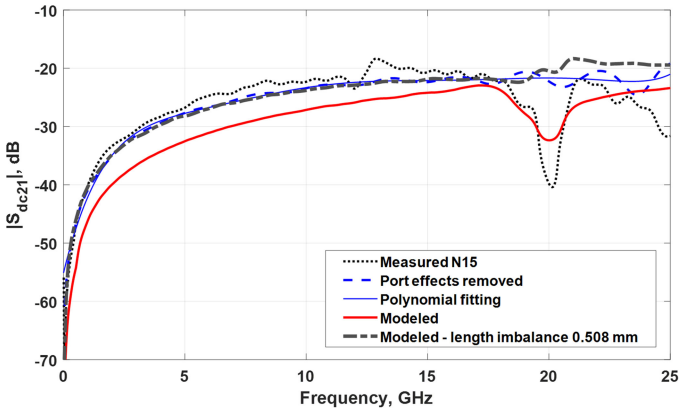

Fig. 12. Measured and modeled magnitude $|S_{dc21}| = |S_{cd21}|$ for CM to DM conversion in one differential pair crossing EBG over 0–25 GHz.

16–23 GHz. The modeled and measured CM notches in Fig. 10 agree closely in shape, position of the resonance frequency, resonance depth, and widths at levels below –15 dB.

The procedure to remove port-related artifacts (via stub and coaxial misalignment effects) has also removed the desirable CM notch. The remaining frequency dependence is close to a linear trend, describes the OFF-resonance IL behavior, and corresponds to the same differential pair, but without any EBG. Fig. 11 shows the measured, modeled, and reconstructed (after de-embedding) CM notch. In the reconstructed CM notch, the OFF-resonance trend that was present in the raw measured data due to port effects was removed. The de-embedding procedure has resulted in the corrected notch shape at the higher-end frequencies, where via stub effect has become substantial, but practically has not changed the basic CM notch filter characteristics.

Mode conversion from CM to DM is identical to the conversion from DM to CM, therefore only $|S_{dc21}|$ frequency characteristics are shown in Fig. 12. One can see that there is a reasonable agreement between the measured and modeled data over the entire frequency range, considering the low mode conversion values, practically below –20 dB, where ±5 dB difference is quite acceptable. The measured and modeled mode conversion trends are similar, with the characteristic dips at ~20 GHz. The modeled results show overall slightly lower mode conversion than the measured. This may be related to the higher length imbalance on a test structure than in a model. The modeled mode conversion could be tuned to the measured value by varying line length imbalance, where 5–20 mil imbalance is quite typical for high-speed differential pairs. Fig. 12 shows that the modeled case with 20-mil length difference in the differential pair captures the measured $|S_{cd21}|$ very well over the entire frequency range. Fig. 12 also contains the mode conversion curve, when port effects were removed; it can be fitted very well by a smooth polynomial of the seventh order.

Note that port effects removal procedure includes the elimination of the wideband via stub effect that is the most pronounced after 15 GHz, where the CM notch appears. The parasitic resonance at around 12–13 GHz due to the TE_{11} mode excitation at the coaxial connector is also removed; however, this resonance

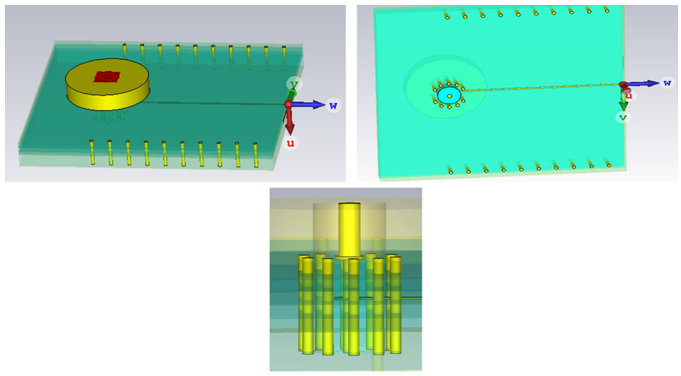

Fig. 13. Views of coaxial connector model with a 50-Ω stripline segment and two waveguide ports and connector pin-to-trace and via structure.

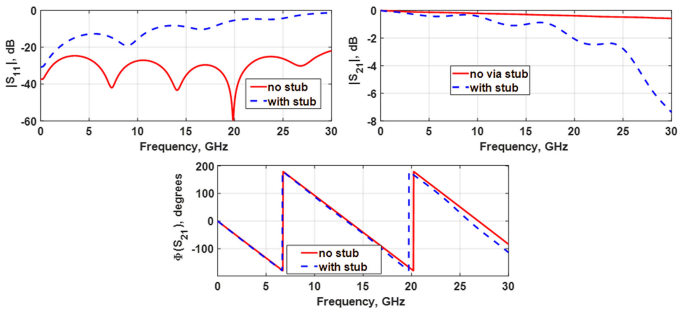

Fig. 14. Modeled *S*-parameters of a 2.92-mm coaxial connector and 10-mm stripline segment, without via stub and with 1.008-mm via stub.

is not that important since it does not affect the 20-GHz CM notch.

The stripline EBG structure N15 was also modeled with additional 2.92-mm SMA connectors. A connector model is illustrated by Fig. 13. The connector has a 10-mm straight 50-Ω stripline segment attached. A via stub (herein, 1.008-mm long, corresponding to the real via stub in the test structure) was modeled. The modeled $|S_{cc21}|$ and $|S_{dd21}|$ for the connector with 10-mm stripline segment with and without via stub are shown in Fig. 14. The via stub clearly deteriorates the connector performance at the higher frequencies.

The cascading procedure in CST Studio was used to attach the connector model to each port of the model N15; the length of the striplines was modified so that the total length structure would be the same as before, 80.4 mm. As is seen in Fig. 15, the modeled results with connectors included are much closer to the measured data than when connectors were not modeled.

The dependencies analogous to those shown for N15 structure have been obtained for all the other structures (N16–N18), showing comparatively good agreement between the modeled and measured results. This gives peace of mind for further numerical experiments that will help to see how the CM filter notch characteristics vary as design parameters vary.

The modeled dependence for the cases of two differential pairs crossing the EBG structure were also validated by measurements. The results are shown in Fig. 16 for CM characteristic over the frequency range 17–23 GHz near the fork-like notch

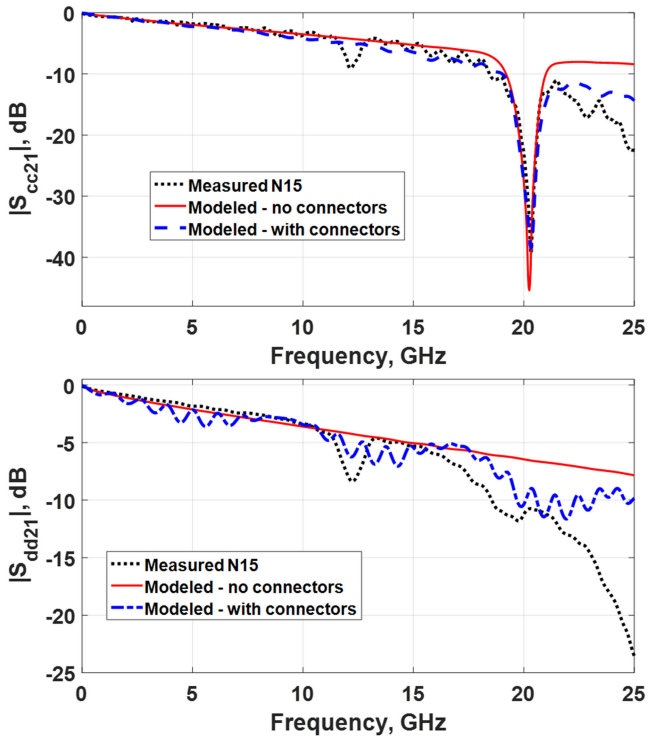

Fig. 15. Measured and modeled mixed-mode IL of CM and DM for N15 structure with and without connectors.

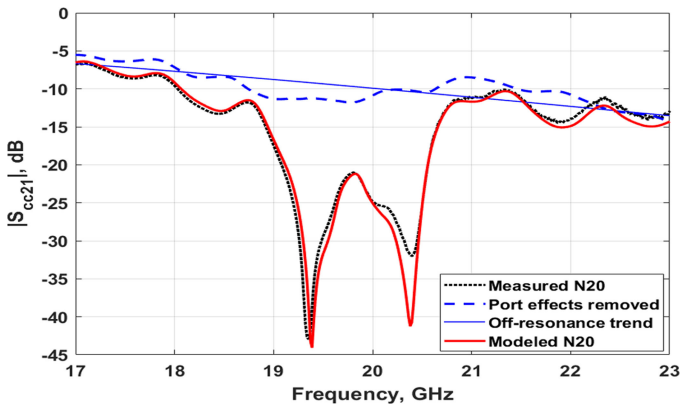

Fig. 16. Measured and modeled magnitude $|S_{cc}21|$ for N20 with two differential pairs crossing EBG.

for the structure N20. The resultant shapes and resonance dips agree well.

The IL for DM is shown in Fig. 17: the original measurement, the corrected IL after port effects removal, and the modeled data. The modeled and measured (after port effects removal) $|S_{dd21}|$ agree well (discrepancy is <0.5 dB) over the entire frequency range.

The measured mode conversion is not treated with port de-embedding; it was applied only to IL for CM and DM. Fig. 18 shows the measured (dotted line) and modeled (solid line) mode conversion frequency dependencies. Overall, mode conversion values below –20 dB may be considered as acceptable; therefore, possible discrepancy between the measured and modeled

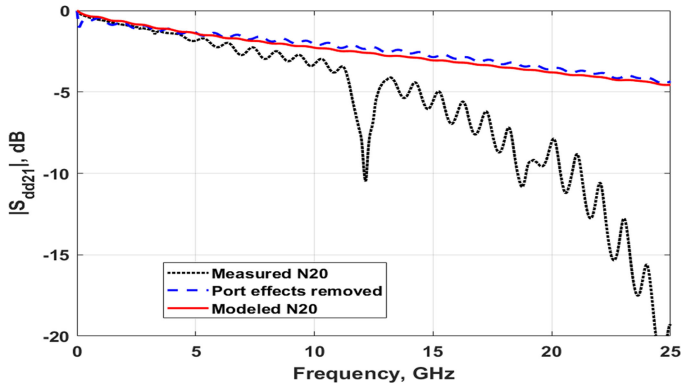

Fig. 17. Measured and modeled magnitude $|S_{dd}21|$ for N20 with two differential pairs crossing EBG.

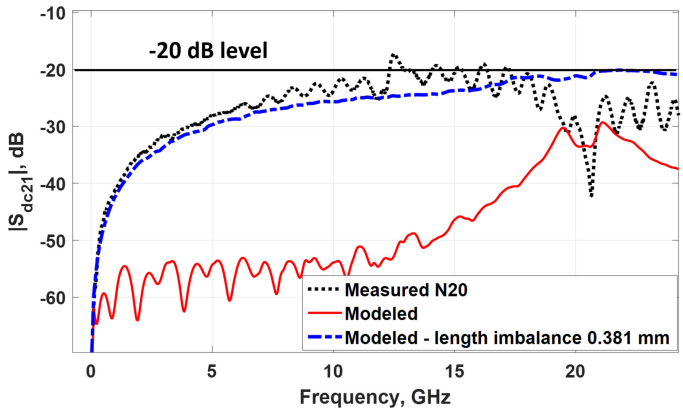

Fig. 18. Measured and modeled magnitude $|S_{dc21}| = |S_{cd21}|$ for N20 with two differential pairs crossing the EBG patch.

results does not matter for the CM filter performance. The discrepancy between the measured and the modeled (solid line) dependencies in Fig. 18 is mainly due to not considering imbalance in the line lengths of the differential pair. This imbalance is known to cause mode conversion enhancement [25], [30]. However, over the region of interest, 17–23 GHz, the modeled and measured mode conversion levels are close, and the dip at ~20 GHz appears on both curves indicating that the EBG structure reduces not only CM, but mode conversion, too. The introduced length imbalance between two lines in the differential pair (15 mil = 0.381 mm) results in the better agreement between the measured and modeled (light dashed line) mode conversion for the frequency range up to 18 GHz.

V. Numerical Experiments With Parameters Variation for EBG Structures

The objective of numerical modeling experiments is not to just optimize parameters of an EBG CM filter according to some performance criteria. The numerical study herein is aimed at capturing trends of EBG CM filter characteristics variations as the functions of the basic design parameters and understanding the physical reasons for these variations. Understanding these physical reasons and constraints should be a guidance for the practical choice of the filter design parameters.

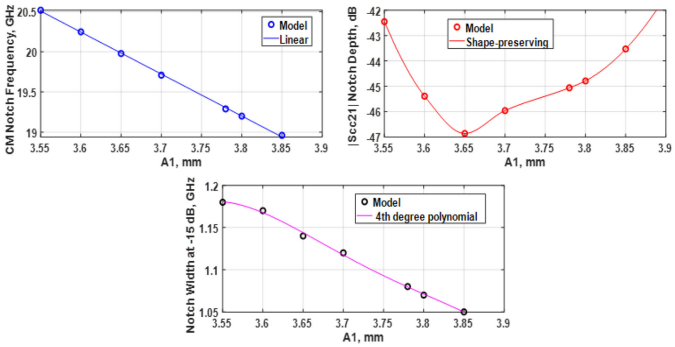

Fig. 19. Dependencies of EBG CM filter parameters on the size of the first patch A_1.

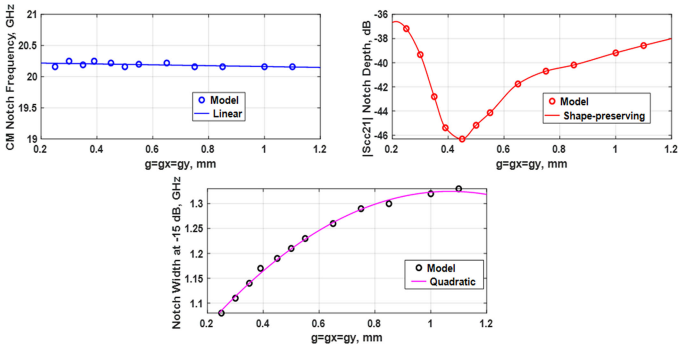

Fig. 20. Dependencies of EBG CM filter parameters on the gap between EBG patches.

A number of numerical experiments were run on the test structure N15 taken as the baseline. These numerical experiments include variations of a number of design parameters and show how the CM notch filter parameters change. The basic parameters of the filters: resonance or center notch frequency of $|S_{cc21}|$; resonance depth (minimum value of $|S_{cc21}|$, dB); and width at the level of –15 dB, are analyzed as functions of various design parameters and technological features. The design parameters herein are the EBG patch dimensions A_{yj}; sizes of gaps between the patches $g_{x,yj}$ (all of them are chosen identical and equal to g); position of the differential lines crossing the EBG with respect to the top edge of the EBG patches *ht*; thicknesses of the dielectric layers $d_{1,2,3}$. The technological features are the ERD layer thickness *tSTD*, assuming that the average peak-to-valley roughness magnitude of STD foil may vary over some range depending on the particular PCB; base angle of the trapezoid cross section of a trace; and line length mismatch in a differential pair.

Fig. 19 shows the dependencies of the EBG CM filter parameters on the *y*-size of the first patch A_1 (the index *y* is omitted here and further), as extracted from numerical modeling results. The dimensions A_2 differ from each A_1 by 0.4 mm, and the dimension A_3 differ from each A_1 by 0.8 mm. It is seen that the CM notch (resonance) frequency varies linearly with *y*-dimension of the first patch in accordance with (1). Maximum depth of the notch, or minimum of $|S_{cc21}|$, dB is achieved at $A_1 = 3.65$ mm, which corresponds to $f_{\rm res} = 20$ GHz. The width of the CM filter notch decreases as the EBG patch size increases.

Computations show that if the differential traces cross the first EBG row, and the *y*-size of the patch A_1 on the first row remains the same, whereas the sizes of the patches A_2 and A_3 in the other two rows vary, the resonance frequency remains practically the same. There is just a slight increase (fraction of a dB) in the $|S_{cc21}|$ at the notch frequency as A_2 and A_3 increase, and the notch width slightly increases. Therefore, the dimensions of the patch that is crossed by the differential pair mainly determine the CM notch filter characteristics.

The dependencies for the CM filter notch frequency, depth, and width at –15 dB on the gap size g are presented in Fig. 20. Note that all gaps varied in unison. Notch frequency is practically independent of the gap size, whereas the notch level is the deepest at around $g = 0.45$ mm. At this gap, there is maximum energy "absorbed" in the EBG cavities. For this reason, in the measured test structures, N15 that has $g = 0.39$ mm has the deepest notch, whereas the structures with $g = 0.25$ mm show the less deep notches. The width of the notch increases monotonically as the gap increases. At the initial part ($g < 0.45$ mm), along with the notch depth increase, this behavior may be associated with the decrease of coupling between the patches, resulting in less distortion of the resonance response. Then, for $g > 0.45$ mm, the quality factor (Q-factor) of the resonance decreases; one of the reasons for that could be the loss of energy stored at the resonance through the gaps. This is true for both DM and CM.

Characteristics of the EBG filters as functions of the distance *ht* between the top of the first EBG patch and the top edge of the first line of the differential pair are shown in Fig. 21. Since these are 2×3 EBG structures, the parameters were extracted for the cases when differential traces cross each of the three EBG rows. It is seen that the notch (resonance) frequency varies within some range with maximum frequency when the signal traces are at the center of the EBG patch in each row. The higher notch frequencies are observed when traces cross the first row, and for the other two rows the frequencies are consequently lower. However, notch frequency variations are not very significant; in the modeled example, the variation is within ~0.6 GHz.

The notch depth values vary substantially, though. The ranges of variations within each EBG row of 2×3 structure are approximately the same, from about –50 dB closer to the patch edges to about –7 dB at the patch centers. Signal traces running over the gaps between the rows are excluded from consideration, since DM would be deteriorated if return plane under the traces is significantly disrupted. Note that there is some depth decrease as the second trace of the differential pair comes very close to the patch edge; in this case, imbalance in a differential pair increases, and these regions should be also excluded from consideration.

As is mentioned in the Introduction, coupling between the signal traces and the patches is minimal at the center and increases towards the patch edges because of the E_z-field distribution is similar to that of $\rm TM_{010}$ mode in a rectangular cavity with magnetic walls [17]. This explains why the CM filter notches are deeper when traces are closer to the patch edges. This is similarly true about the width of the EBG notch. When traces run close to

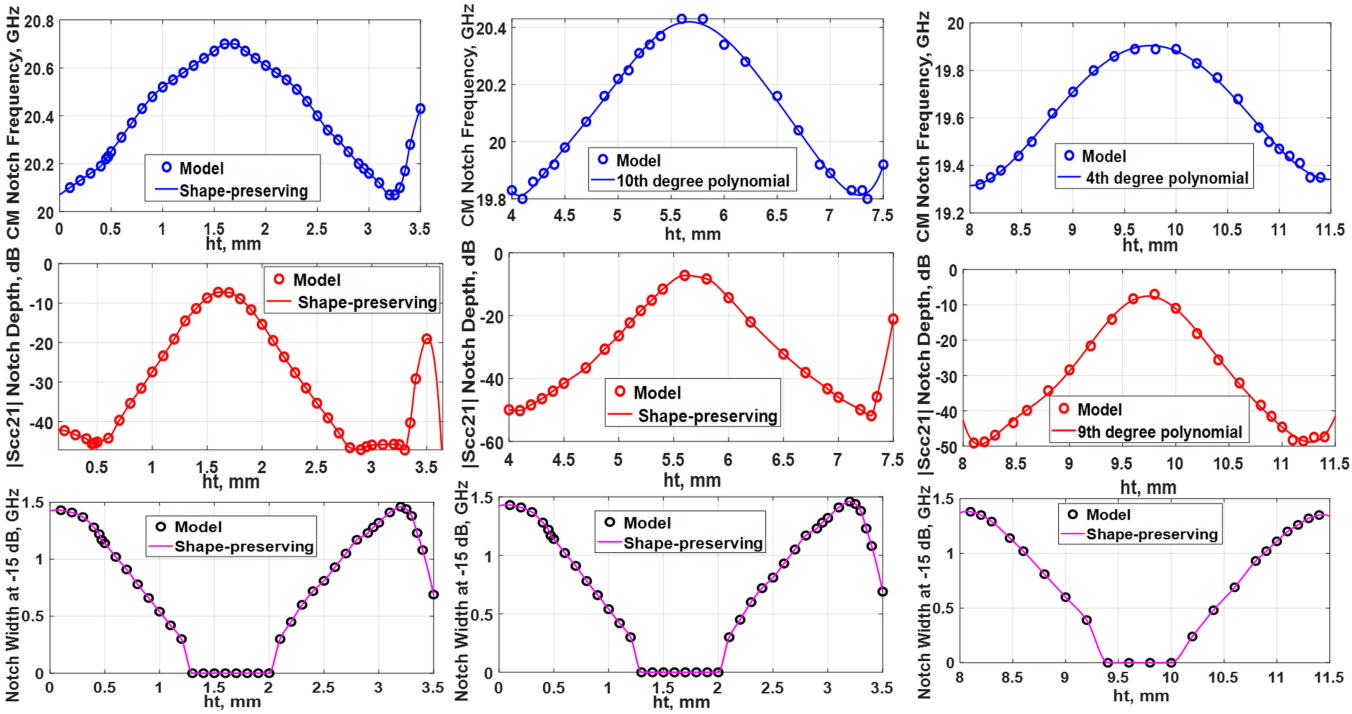

Fig. 21. Dependencies of 2 × 3 stripline EBG CM filter characteristics on the distance *ht*.

the center, the notch depth is above –15 dB; this corresponds to a zero-value set in a notch width curve. The notch width increases towards the patch edges, where EBG patch cavity excitation is the most efficient.

The best performance of the EBG stripline structure from the point of view of the notch depth should be when traces run at least 10% of A_{yj} away from the EBG patch edges. They should not run too close to the center where the electric field of TM_{010} mode is minimum. In the baseline filter N15, the distance $ht = 0.472$ mm, and this is close to the optimum position of the traces in the stripline EBG filter.

The next series of numerical experiments are variations of thickness of the dielectric layers in the EBG filter stackup, *d1*, *d2*, and *d3* (one thickness parameter was varied at a time). Though variations of the layer thicknesses *d1* and *d2* affect impedances of the lines and may cause undesirable DM propagation mismatches, it is still useful to know how CM filter parameters change. Variation of *d3*, the thickness of the dielectric layer beneath the EBG structure, may be a degree of freedom for CM filter design, even though this thickness is too low to allows for any electromagnetic field variation within it.

As is seen in Fig. 22, the CM notch frequency gradually shifts to the higher frequencies as thickness *d1* (between the stripline and EBG planes) increases. By increasing *d1,* coupling of the CM from the signal traces to the cavities beneath the EBG (of thickness *d3*) reduces, the apparent loss in the cavity decreases, the corresponding resonance becomes sharper, and shifts to the higher frequencies, but due to the reduced coupling its depth reduces.

However, there is a decrease of the resonance frequency with the increase of both *d2* (above the stripline) and *d3* (between the EBG and the lower ground plane). The resonant frequency

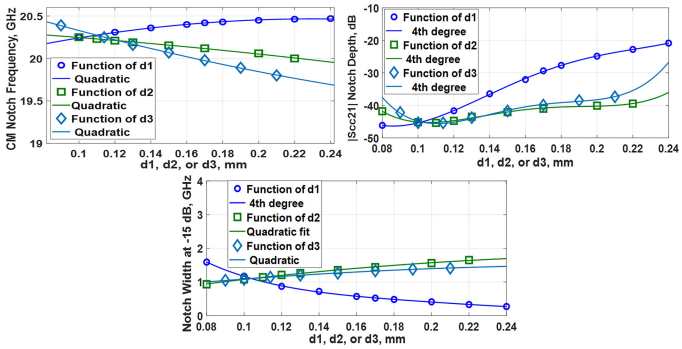

Fig. 22. Dependencies of 2 × 3 EBG CM filter characteristics on the thicknesses *d1, d2*, and *d3*.

decreases with the larger *d3*, because the fringing fields extend further making the effective size of the patch larger. Also, the thicker dielectrics *d2* and *d3* may "load" the EBG cavities more, causing both reduction of the notch frequency and increase of its width.

The CM notches in all the cases are the deepest when impedances are close to $Z_{DM} = 100\,\Omega$ and $Z_{CM} = 25\,\Omega$, i.e., like $d1 = 0.1$ mm and $d2 = 0.11$ mm in N15 structure. There are EBG cavities between the EBG plane and the ground plane, and the thickness of dielectric layer *d3* should match thicknesses *d1* and *d2* to provide the maximum depth of the CM filter notch. The width of the notch should be correlated with its depth, and as width drops with *d1* increase, it is undesirable to have it different from the nominal case with $Z_{DM} = 100\,\Omega$ and $Z_{CM} = 25\,\Omega$.

Dielectric properties, in particular, dielectric constant (*DK*) of substrates in the stackup, were also varied. It is assumed that all the layers have identical dielectric properties (though core and

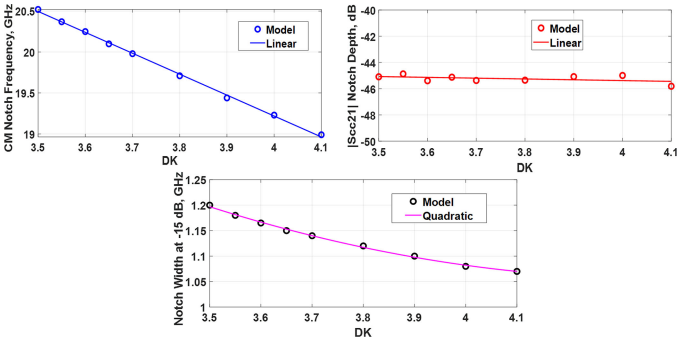

Fig. 23. Dependencies of 2 × 3 EBG CM filter characteristics on dielectric constant DK of the PCB substrates.

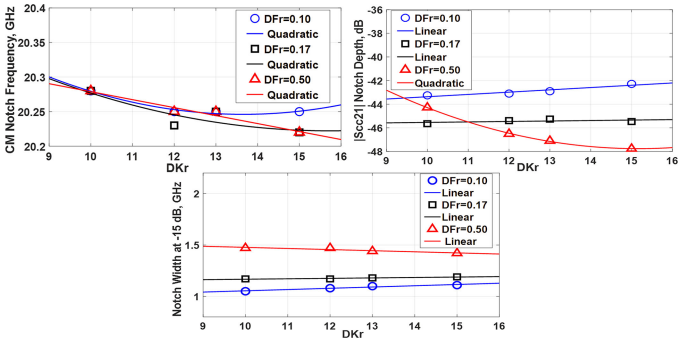

Fig. 25. Dependencies of 2 × 3 EBG CM filter characteristics on ERD layer parameters for STD copper foil, ERD layer thickness tSTD = 12.4 μm.

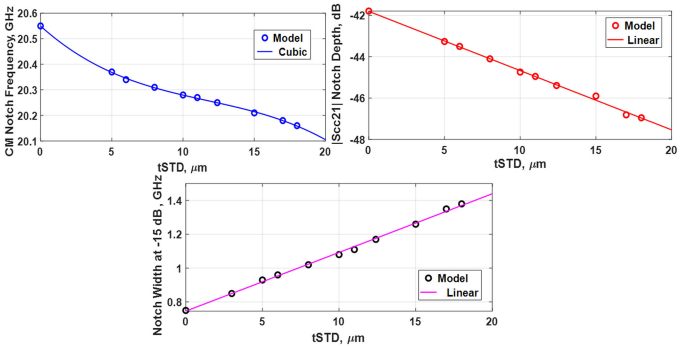

Fig. 24. Dependencies of 2 × 3 EBG CM filter characteristics on the thickness of ERD layer for STD copper foil.

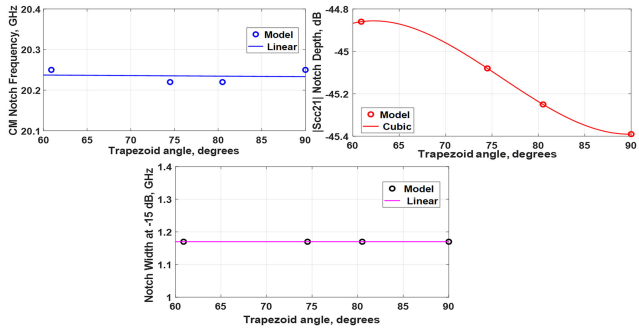

Fig. 26. Dependencies of 2 × 3 EBG CM filter parameters on the base angle of the trapezoid shape of the signal trace cross section.

prepreg dielectrics may slightly differ in a real PCB stackup). In this test case, dielectric layers were set in the numerical models as dielectrics with constant parameters. *DK* varied as a parameter, and loss tangent was kept the same. This was done for simplicity and expediting simulations. The case with $DK = 3.60$ and $DF = 0.0073$ at 35 GHz (constant fit setting in CST) is very close to Megtron 6 frequency-dispersive case.

The numerical experiments illustrated by Fig. 23 show that CM filter notch frequency reduces linearly as *DK* increases, and this is consistent with (1). *DK* is one of the degrees of freedom to control CM notch frequency, along with the patch size, unless the PCB properties are pre-determined before the design and fixed. Notch depth practically does not change with *DK* variation; this is because *DK* affects phase relations rather than loss. CM notch width reduces as *DK* increases and the notch moves towards the lower frequencies.

Note that the *DK* value and dielectric thicknesses may affect impedance matching between the differential pair above the EBG structure and the neighboring components on the PCB, e.g., connectors. Therefore, deviation from the nominal values of impedances, e.g., $Z_{DM} = 100\,\Omega$ and $Z_{CM} = 25\,\Omega$, is undesirable, since mismatches may deteriorate the CM filter performance.

Fig. 24 shows the CM filter characteristics as functions of the ERD layer thickness, *tSTD*. The effective roughness dielectric parameters, *DKr* and *DFr*, in this experiment remain the same, $DKr = 12$ and $DFr = 0.17$. As *tSTD* increases, the CM notch frequency shifts to the lower frequencies. Consequently, the notch depth increases, and the resonance line becomes wider, as the ERD layer plays the part of the cavity loading, therefore, the overall loss increases.

For different copper foil roughness values, not only ERD layer thicknesses are different, but effective roughness dielectric parameters, *DKr* and *DFr*, are different, too [25]. Therefore, in the numerical experiments, the ERD parameters are varied, whereas keeping thickness the same, $tSTD = 12.4$ μm. The results are shown in Fig. 25. There is no significant impact on the CM filter notch frequency, when *DKr* varies from 10 to 15. There is a slight variation of the notch depth, but it depends on the *DFr* value. Width of the notch also does not depend much on the *DKr*; however, it depends on the *DFr* value.

In this paper, we also studied the effects of the trapezoid shape of the traces. The dependencies of the CM filter parameters as functions of the trapezoid base angle are shown in Fig. 26. It is seen that the trapezoid shape of traces does not change CM notch filter parameters, except for the slight reduction of the notch depth as angle decreases (a rectangular trace has 90° angle). However, the sharper angle may result in the higher IL for DM, and in some cases may cause enhanced mode conversion, similar to what was noticed for the structures without EBG [17], [24] and for EBG microstrip structures [29].

Adding line length imbalance in the differential pair will cause an increased mode conversion. This is illustrated by Figs. 12 and 27 for N15 case. The other characteristics of the filter (notch resonance frequency, depth, and width) remain practically the same as the line length imbalance varies.

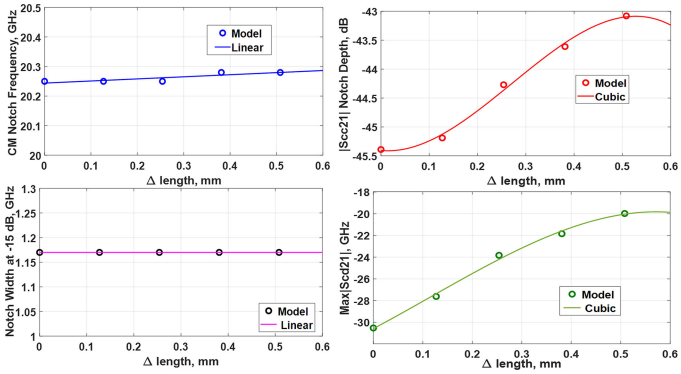

Fig. 27. Dependencies of 2×3 EBG CM filter parameters on length mismatch for the lines of the differential pair.

VI. Conclusion

A workflow of EBG CM stripline notch filter design, its physical peculiarities and sensitivities to various technological geometrical and material parameters are discussed in this paper. Modeling, design, and experimental characterization of a number of 20-GHz stripline EBG filters with one or two stripline differential pairs are presented. The corresponding full-wave numerical models take into account various technological features and their relative weight in the EBG filter behavior and show good agreement with the measurements. Systematic analysis using the variation of different design parameters was done, and the obtained trends of filter characteristic behavior can be useful for the optimal design of stripline EBG filters with rectangular patches.

The presented design methodology can be used to design CM notch filters for other frequencies and for more than two differential pairs crossing the EBG structure. If multiple notches are needed, patches allowing for the corresponding number of field variations in either or both *x*- and *y*-direction over the desirable frequency range can be used.

References

[1] M. J. Hill, R. W. Ziolkowski, and J. Papapolymerou, "Simulated and measured results from a duroid-based planar MBG cavity resonator filter," *IEEE Microw. Guided Wave Lett.*, vol. 10, no. 12, pp. 528–530, Dec. 2000.

[2] A. Oliner, "Periodic structures and photonic-band-gap terminology: Historical retrospectives," in *Proc. 29th Eur. Microw. Conf.*, vol. 3, Munich, Germany, Oct. 1999, pp. 295–298.

[3] E. Yablonovich, T. G. Gmitter, and K. M. Leung, "Photonic band structure: The face-centered-cubic case employing non-spherical atoms," *Phys. Rev. Lett.*, vol. 67, no. 17, pp. 2295–2298, Oct. 1991.

[4] D. Sievenpiper and E. Yablonovich, "Eliminating surface currents with metallodielectric photonic crystals," in *Proc. IEEE MTT-S Int. Symp. Microw. Symp. Dig.*, Jun. 1998, Paper WE3A-6.

[5] D. Sievenpiper, L. Zhang, R. F. J. Boras, N. G. Alexopolous, and E. Yablonovitch, "High-Impedance electromagnetic surfaces with forbidden frequency band," *IEEE Trans. Microw. Theory Techn.*, vol. 47, no. 11, pp. 2059–2074, Nov. 1999.

[6] G. Parker and M. Charlton, "Photonic crystals," *Phys. World*, vol. 13, pp. 29–34, Aug. 2000.

[7] H. F. Shaban, H. A. Elmikaty, and A. A. Shaalan, "Study the effects of electromagnetic band-gap (EBG) substrate on two patches microstrip antenna," *PIER B*, vol. 10, pp. 55–74, 2008.

[8] A. Orlandi, B. Archambeault, F. de Paulis, and S. Connor, *Electromagnetic Bandgap (EBG) Structures: Common Mode Filters for High Speed Digital Systems*. New York, NY, USA: Wiley-IEEE Press, 2017.

[9] T.-L. Wu, C.-H. Tsai, T.-L. Wu, and T. Itoh, "A novel wideband common-mode suppression filter for gigahertz differential signals using coupled patterned ground structures," *IEEE Trans. Microw. Theory Techn.*, vol. 57, no. 4, pp. 848–855, Apr. 2009.

[10] C.-Y. Hsiao, C.-H. Tsai, C.-N. Chiu, and T.-L. Wu, "Radiation suppression for cable-attached packages using a compact embedded common-mode filter," *IEEE Trans. Compon., Packag., Manuf. Techn.*, vol. 2, no. 10, pp. 1696–1703, Oct. 2012.

[11] W.-T. Liu, C.-H. Tsai, T.-W. Han, and T.-L. Wu, "An embedded common-mode suppression filter for GHz differential signals using periodic defected ground plane," *IEEE Microw. Wireless Compon. Lett.*, vol. 18, no. 4, pp. 248–250, Apr. 2008.

[12] F. de Paulis, B. Archambeault, M. H. Nisanci, S. Connor, and A. Orlandi, "Miniaturization of common mode filter based on EBG patch resonance," in *Proc. IEC DesignCon*, vol. 3, 2012, pp. 2320–2338.

[13] F. De Paulis, L. Raimondo, D. Di Febo, B. Archambeault, S. Connor, and A. Orlandi, "Experimental validation of common-mode filtering performances of planar electromagnetic band-gap structures," in *Proc. IEEE Int. Symp. Electromagn. Compat.*, Fort Lauderdale, FL, USA, Jul. 25–30, 2010, pp. 764–769.

[14] W. Wang, X.-Y. Cao, R. Wang, and J.-J. Ma, "A small dual-band EBG structure for microwave," in *Proc. Int. Conf. Microw. Millimeter Wave Technol.*, Nanjing, China, Apr. 2008, pp. 1637–1639.

[15] M. Pajovich, J. Savic, A. Bhobe, and X. Zhou, "The gigahertz two-band common-mode filter for 10-Gbit/s differential signal lines," in *Proc. IEEE Symp. Electromagn. Compat.*, Denver, CO, USA, Aug. 5–9, 2013, pp. 472–477.

[16] C. A. Balanis, *Advanced Engineering Electromagnetics*. New York, NY, USA: Wiley, 1989, sec. 8.3.

[17] C. A. Balanis, "Microstrip antennas," *in Antenna Theory: Analysis and Design*. 3rd ed., Hoboken, NJ, USA: Wiley, 2005, pp. 812–835, ch. 14.

[18] M. Koledintseva, S. Radu, and J. Nuebel, "Physical and technological aspects of microstrip EBG filter design," in *Proc. IEEE Int. Symp. Electromagn. Compat., Signal Integrity Power Integrity*, Long Beach, CA, USA, Jul. 30–Aug. 3, 2018, pp. 211–216.

[19] Q. Liu *et al.*, "Reduction of EMI due to common-mode currents using a surface-mount EBG-based filters," *IEEE Trans. Electromagn. Compat.*, vol. 58, no. 5, pp. 1440–1447, Oct. 2016.

[20] F. de Paulis *et al.*, "EBG-based common-mode microstrip and stripline filters: Experimental investigation of performances and crosstalk," *IEEE Trans. Electromagn. Compat.*, vol. 57, no. 5, pp. 996–1004, Oct. 2015.

[21] F. de Paulis, M. Cracraft, C. Olivieri, S. Connor, A. Orlandi, and B. Archambeault, "EBG-Based common-mode stripline filters: Experimental investigation on interlayer crosstalk," *IEEE Trans. Electromagn. Compat.*, vol. 57, no. 6, pp. 1416–1424, Dec. 2015.

[22] I. Arnedo *et al.*, "Analytical solution for the design of planar EBG structures with spurious-free frequency response," in *Proc. 39th Eur. Microw. Conf.*, Rome, Italy, Oct. 2009, pp. 1299–1302.

[23] A. A. Andronow and C. E. Chaikin, *Theory of Oscillations*. Princeton, NJ, USA: Princeton Univ. Press, 1949.

[24] CST Studio Suite, Dassault Systems Simulia, 2017. [Online]. Available: www.cst.com

[25] M. Koledintseva, T. Vincent, and S. Radu, "Full-Wave simulation of an imbalanced differential microstrip line with conductor surface roughness," in *Proc. IEEE Symp. Electromagn. Compat. Signal Integrity*, Santa Clara, CA, USA, Mar. 15–20, 2015, pp. 34–39.

[26] M. Koledintseva, T. Vincent, A. Ciccomancini Scogna, and S. Hinaga, "Method of effective roughness dielectric in a PCB: Measurement and full-wave simulation verification," *IEEE Trans. Electromagn. Compat.*, vol. 57, no. 4, pp. 807–814, Aug. 2015.

[27] D. A. Petrov, K. N. Rozanov, and M. Y. Koledintseva, "Influence of higher-order modes in coaxial waveguide on measurements of material parameters," in *Proc. IEEE Int. Symp. Electromagn. Compat., Signal Integrity Power Integrity*, Long Beach, CA, USA, Jul. 30–Aug. 3, 2018, pp. 66–70.

[28] M. Bailey, "Guidance on selecting and handling coaxial RF connectors used with Rohde & Schwarz test equipment," Rohde & Schwarz, Munich, Germany, Appl. Note, 4.2015-1MA99-2e, Apr. 2015. [Online]. Available: http://www.rohde-schwarz.com/appnote/1MA99

[29] Agilent Technologies, "Differential S-parameters measurements of PCI express connector using ENA series network analyzer," Appl. Note 1463-3, Santa Clara, CA, USA, Jul. 2003.

[30] M. Y. Koledintseva and T. Vincent, "Comparison of mixed-mode S-parameters in weak and strong coupled differential pairs," in *Proc. IEEE Symp. Electromagn. Compat., Signal Integrity Power Integrity*, Ottawa, ON, Canada, Jul. 25–30, 2016, pp. 610–615.

Marina Y. Koledintseva (M'95–SM'03) received the M.S. and Ph.D. degrees from Moscow Power Engineering Institute—National Research University, Moscow, Russia, in 1984 and 1996, respectively.

From 1996 to 2000, she was a Research Scientist and Associate Professor with the National Research University. From January 2000 to April 2004, she was a Research Professor of Electrical Engineering with the Missouri University of Science and Technology (former UMR). From 2014 to 2018, she was a Principal Hardware Design Engineer with the Electromagnetic Compatibility Group, Oracle Corporation, Santa Clara, CA, USA. In September 2018, she joined Metamagnetics, Inc., Westborough, MA, USA, as a Technical Director of Research and Development. She is an author of about 250 publications, including book chapters, peer-reviewed journal articles, international symposia and conference proceedings, and seven inventions. Her research interests include electromagnetic compatibility and signal integrity in electronic systems; computational electromagnetics, development of analytical and numerical models and experimental methodologies to study complex electromagnetic structures and advanced materials, and using various physical phenomena in materials to design new microwave devices, including microwave magnetic ICs.

Dr. Koledintseva has been the winner of numerous Best Paper Awards of international symposia and journals, including the IPC APEX EXPO Best Technical Paper Award in 2009, 2010, and 2018, IEEE Transaction on EMC Honorable Paper Mention Award in 2015, and IEEE EMC Symposium Best Paper Award in 2012 and 2014. From 2007 to 2010, she was a Secretary of Technical Committee TC-11 "Nanotechnology and Advanced Materials" of IEEE EMC-S. From 2010 to 2014, he was a Chair of TC-11, and since 2018 she has been the Vice-Chair of TC-11.

Sergiu Radu (M'93–SM'02) received the M.S. and Ph.D. degrees in electrical engineering (electronics) from the Technical University of Iasi, Iasi, Romania, in 1980 and 1995, respectively.

He was an Associate Professor with the Technical University of Iasi until 1996, involved in electromagnetic compatibility teaching and research. From 1996 to 1998, he was a Visiting Scholar with the Electromagnetic Compatibility Laboratory, University of Missouri at Rolla, currently Missouri University of Science and Technology. In 1998, he was with the Electromagnetic Compatibility Engineering Group, Sun Microsystems, which became a part of Oracle Corporation, Santa Clara, CA, USA, in 2010. He is currently the Director of Hardware Development with Oracle Corporation leading the EMC Design Group, involved in chassis level, PCB level, and chip-level EMC design for all Oracle hardware products. His role also includes the development and implementation of platform level EMC design architecture, design methodologies, and better EMC prediction techniques. He holds seven U.S. patents for EMI reduction techniques in electronic systems and has been the author or coauthor of more than 50 technical papers, presentations, and reports on electromagnetic compatibility related subjects.

Dr. Radu has been a NARTE-Certified Engineer since February 1998, a former IEEE EMC Distinguished Lecturer (2009–2010), and a Reviewer for the IEEE TRANSACTIONS ON ELECTROMAGNETIC COMPATIBILITY.

Joseph Nuebel (M'95) received the AASEE degree in electrical engineering from the Hawkeye Institute of Technology, Waterloo, IA, USA, in 1978.

For the past 32 years, he has been working with Sun Microsystems, Santa Clara, CA, USA, and then Oracle Corporation, Santa Clara, CA (as Sun became a part of Oracle Corporation in 2010) first in the Compliance Department and then in the EMC Hardware Design Group. He is currently a Principal Hardware Engineer at EMC design with Oracle Corporation. His EMC product design contribution has included everything from high-speed switches and large multi-socket servers to disk drives and PCIe cards.